In-situ Construction of Gradient Oxygen Release Buffer and Interface Cation Self-Accelerator Stabilizing High-Voltage Ni-rich Cathode

Zhongsheng Dai, Huiling Zhao, Weixin Chen, Qi Zhang, Xiaosheng Song, Guanjie He, Yong Zhao, Xia Lu, and Ying Bai**

Z. S. Dai, H. L. Zhao, Y. Bai

International Joint Research Laboratory of New Energy Materials and Devices of Henan Province, School of Physics and Electronics, Academy for Advanced Interdisciplinary Studies, Henan University, Kaifeng, 475004, P. R. China

*Corresponding author. E-mail: zhao@henu.edu.cn (H. L. Zhao); ybai@henu.edu.cn (Y. Bai)

W. X. Chen, X. Lu

School of Materials, Sun Yat-sen University, Guangzhou, 510006, P. R. China

Q. Zhang, X. S. Song, Y. Zhao

Key Lab for Special Functional Materials of Ministry of Education, National & Local Joint Engineering Research Center for High-efficiency Display and Lighting Technology, School of Materials Science and Engineering, Collaborative Innovation Center of Nano Functional Materials and Applications, Henan University, Kaifeng, 475004, P. R. China

G. J. He

Department of Chemical Engineering, University College London (UCL), London, WC1E 7JE, UK

Keywords: oxygen release, in-situ construction, stress-strain, structural and electrochemical stabilities, Ni-rich cathodes

Abstract: Ni-rich cathodes with superior energy densities have spurred extensive attention for Lithium-ion batteries (LIBs), whereas their commercialization is hampered by structural degradation, thermal runaway and dramatic capacity fading. Herein, boron (B) with high binding energy to oxygen (O) is gradiently incorporated into each primary particle and piezoelectric $Li_2B_4O_7$ (LBO) is homogeneously deposited on the secondary particles of polycrystalline $LiNi_{0.8}Co_{0.1}Mn_{0.1}O_2$ (NCM811) surface through a facile in-situ construction strategy, intending to synchronously enhance electrochemical stabilities and Li^+ kinetics upon

cycling. Particularly, the as-obtained LBO modified NCM811 cathode exhibits an excellent capacity retention (88.9% after 300 cycles, 1 C) and rate performance (112.2 mAh g^{-1}, 10 C) with Li metal anode, the NCM811-LBO/$Li_4Ti_5O_{12}$ full cell achieves a capacity retention of 92.6% after 1000 cycles (0.5 C). Intensive explorations in theoretical calculation, multi-scale in/ex-situ characterization and finite element analysis ascertain that the improvement mechanism of LBO modification can be attributed to the synergistic contributions of rational designed O release buffer and interface cation self-accelerator. This work provides a facile and practical method to prevent structural degradation and thermal runaway for high-energy LIBs.

1. Introduction

Safe and sustainable high-energy cathodes are indispensable for the development of next-generation lithium-ion batteries (LIBs) in a broad range of practical applications, such as the commercial deployment of electric vehicles (EVs).[1] Particularly, Ni-rich layered oxides $LiNi_xCo_yMn_{1-x-y}O_2$ ($x > 0.6$) are currently employed as power supplies for EVs owing to their superior discharge capacity (> 200 mAh g^{-1}), high output voltage (3.8 V) and environmentally friend characteristics.[2] Nevertheless, the commercial polycrystalline Ni-rich cathodes, generally experience anisotropic lattice variation upon cycling, which could result in the generation of lattice stress and the formation of microcracks, inevitably aggravating detrimental side reactions and finally exacerbating the structural degradation as well as the performance decay.[3] From the electronic structure perspective, the t_{2g} band of $Co^{3+/4+}$ is almost overlapped with the top of O^{2-} 2*p*, thus the oxidation of Co^{3+} under high-potential (> 4.3 V *vs.* Li/Li^+) will be accompanied with the escape of lattice O.[4] Additionally, the electrons located at e_g orbitals of high-valence transition metal cations (TM, Ni^{4+} in particular) in highly delithiated cathodes spontaneously transfer to the 2*p* orbital of lattice oxygen, further aggravate the release of lattice O.[5] The O escape could bring in the migration of TM cations to neighboring Li slabs, resulting in phase transformation from layered to spinel structures, which blocks Li^+ diffusion and thus incurs poor electrochemical performance.[6] Even worse, the released O_2 will react violently with organic electrolytes, leading to severe thermal runaway.[7] It has been reported that the lattice O escape in Ni-rich materials might be

intensified from interior to surface.[8] Accordingly, the stability of cathode-electrolyte interface and bulk crystal structure should be systematically considered to develop safe, high energy density and longevity Ni-rich materials.[9]

Substantial efforts have been made to subdue the aforementioned issues and improve the cycling stability of Ni-rich cathodes, wherein surface coating and doping heteroatoms with high binding energies to lattice O could effectively ameliorate the anisotropic strain accumulation and O_2 segregation in Ni-rich cathodes.[10] Typically, NASICON-type $Li_{1.4}Y_{0.4}Ti_{1.6}PO_4$[11] and inert Al_2O_3[12] coating layers have been utilized to stabilize the structure of Ni-rich particles through alleviating stress accumulation and suppressing surface side reactions, which were found to be easily exfoliated from bulk materials upon cycling due to weak interaction, high lattice mismatch and dramatic anisotropic lattice contraction along the crystallographic *c*-axis.[13] Furthermore, surface coating cannot fundamentally address the awkward situation of microcracks inside secondary particles.[14] Once the crack penetrates through the encapsulation layer, the electrolyte will further impregnate among the secondary particles, eventually deteriorating the crack and leading to structural collapse. To stabilize lattice O and crystal texture, heteroatom doping (*e.g.*, Mg^{2+}, Ti^{4+}) has been employed to alleviate O_2 release and improve the structural stability through regulating O^{2-} 2*p* bands,[15] simultaneously restraining microcracks upon cycling. Unfortunately, the proposed incorporated atoms were generally found to occupy the active Li^+ or TM cation sites, resulting in obvious capacity decay.[16] Moreover, conventional modification strategies could only dope heteroatoms into the peripheral surface of secondary particles, which inhibit the contribution of heteroatom doping to a large extent in structural stabilization from alleviating O escape and microcracks growth.[17] Therefore, appropriate modification of materials and synthetic approaches are desiderated to address the stability concerns, including lattice O escape and stress-strain accumulation, aiming at eventually enhancing the cyclability of Ni-rich materials for LIBs.

In this work, through an in-situ construction method (described in the Materials synthesis section), boron (B) with high binding energy to O (B─O: 809 kJ mol^{-1}) was gradiently incorporated into each primary particle and piezoelectric $Li_2B_4O_7$ (LBO, with a superior

piezoelectric coefficient of 8.76 pC N^{-1} and ionic conductivity of 10^{-5} cm^2 s^{-1}) was simultaneously decorated on the secondary particles of $LiNi_{0.8}Co_{0.1}Mn_{0.1}O_2$ (denoted as NCM811-LBO) surface. The influence of B ion-doping on Ni-rich cathode has been hotly debated over the years, whereas the in-depth understanding is urgent to be established. Herein, based on intensive in-situ/ex-situ experimental investigations and calculations, the doping site of B cations in Ni-rich material and its effect on stabilizing lattice structure were comprehensively illuminated. The calculation results demonstrated for the first time that the B cations were inclined to be incorporated into the tetrahedral site of Li layer, forming strong covalent B─O bonds with adjacent O atoms, thus enhancing the O atom electronegativity to resist excessive oxidation during high-voltage charge compensation. Moreover, as a typical piezoelectric material, the deposited LBO compound effectively accelerated interfacial Li^+ diffusion kinetics through introducing a local polarization electric field upon cycling. Theoretical calculation and finite element analysis further elucidated a reduced energy barrier for ion diffusion and weakened stress accumulation through B^{3+} gradient incorporation and LBO surface modification on NCM811. The as-obtained LBO modified NCM811 cathode exhibits an excellent capacity retention (88.9% after 300 cycles, 1 C) and rate performance (112.2 mAh g^{-1}, 10 C) with Li metal anode. Furthermore, the NC811-LBO/$Li_4Ti_5O_{12}$ full cell achieved 92.6% capacity retention after 1000 cycles under 0.5 C. This work not only provides a facile and pragmatic strategy for constructing uniform coating with superb structural compatibility and stability, but also opens up a new avenue to suppress the oxygen release in ultra-high voltage Ni-rich cathodes.

2. Results and Discussion

To elucidate the influence of B-doping on lattice O in Ni-rich sample, a detailed theoretical analysis was carried out and the corresponding results were demonstrated in **Figure 1**, Figure S1 (Supporting Information) and Table S1-3 (Supporting Information). Typically, a 3*a* × 3*b* × 1*c* supercell of O3-$LiNi_{0.8}Co_{0.1}Mn_{0.1}O_2$ was employed as the structural model for density functional theory (DFT) calculations and the atoms permutation was illuminated in Figure S1a (Supporting Information). Previous reports have alleged that the B cations was more apt to being incorporated into the tetrahedral sites, forming BO_4 tetrahedral or BO_3 triangular

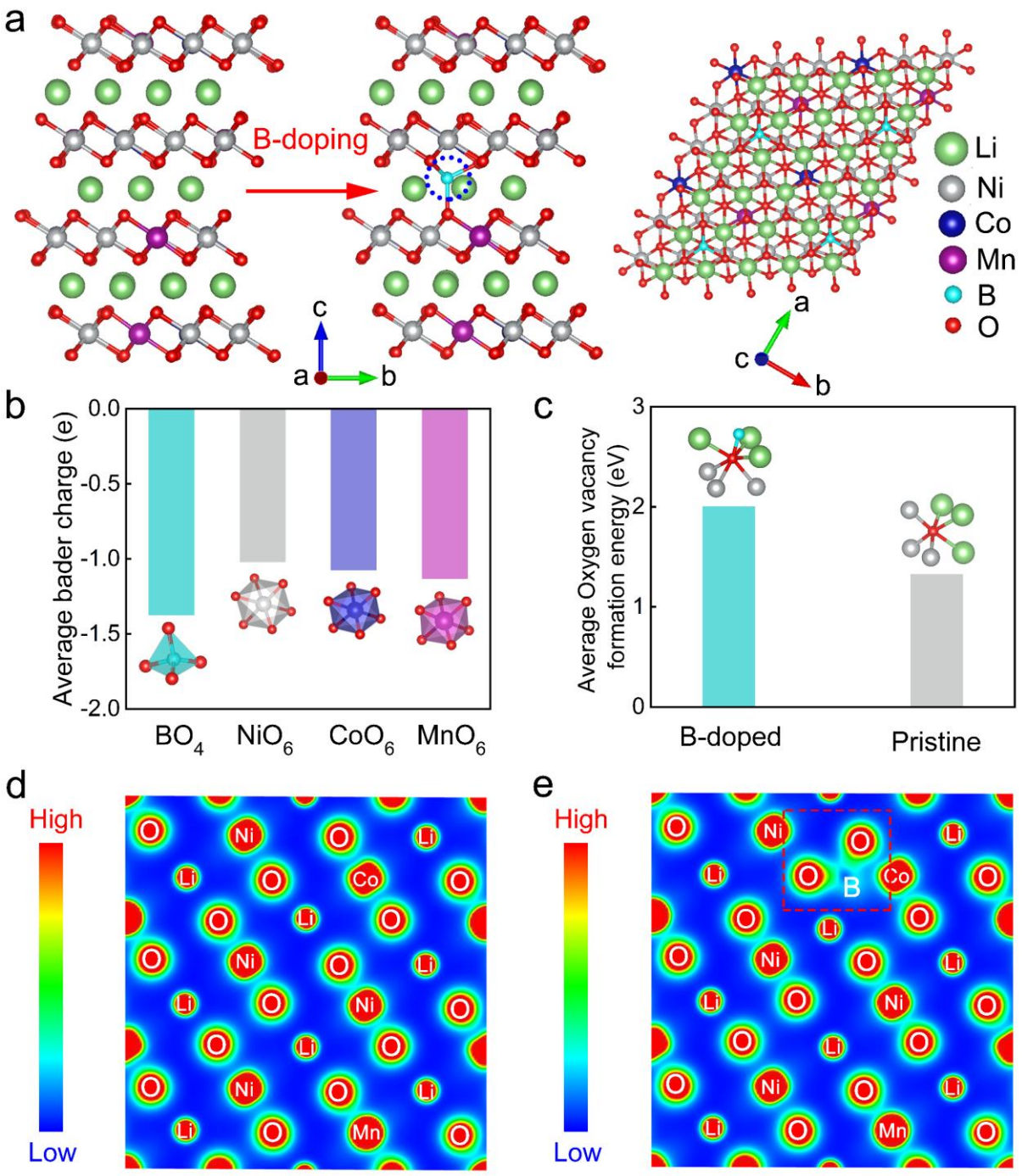

Figure 1. (a) Schematic crystalline structures of NCM811 and NCM811-LBO; (b) average Bader charge of O atom in BO_4 tetrahedron and MO_6 octahedrons (M = Ni, Co, Mn); (c) average oxygen vacancy formation energy; contour maps of charge density in (d) NCM811 and (e) NCM811-LBO.

configurations,[18] whereas the details remained ambiguous. According to the calculation results displayed in Figure S1b (Supporting Information) and Table S1 (Supporting Information), it was clear that the lattice structure with B-doping into Li layer tetrahedron

surrounded by Li-Li-Li-Co was more stable than others. Bader charge analysis was applied to ascertain the influence of B-doping on the Ni-rich microstructure (Figure 1b; Table S2, Supporting Information). The average charge nearby O atoms in BO_4 tetrahedron was more negative than those in NiO_6, CoO_6 and MnO_6 octahedron. This signified that each B─O bond introduced more negative charge for O atom (~ − 0.3 e), which was available to stabilize the O ligand framework, thus resisting excessive O escape during high-voltage charge.

The O vacancy formation energies of pristine NCM811 and NCM811-LBO samples were further quantified to disclose the stabilizing effect of B-doping on lattice O. The corresponding results illustrated in Figure 1c and Table S3 (Supporting Information) clearly manifested that an increased energy value of 0.5 eV with the incorporation of B element into Li^+ slab, indicating that lattice O was more difficult to escape from crystalline structure.[19] Additionally, an obvious stronger B─O covalent bond with introducing extra electrons for the O atom appeared in the modified samples according to charge density analysis (Figure 1d, e), coinciding with the Bader charge analysis. The calculation analysis herein provided solid evidence that the B-doping could effectively suppress the escape of lattice O. Moreover, the B doping in specific site (tetrahedral position in lithium layer) has been confirmed to serve as pillars in stabilizing the crystal structure of layered active materials in highly delithiated state, clearly supporting the previous assumption that B-doping suppressed lattice collapse of Ni-rich cathodes during H2→H3 phase transition.[20]

The in-situ modification strategy to modified NCM811 cathode with LBO through a facile one-step annealing approach is illustrated in Figure 2a. Figure S2 (Supporting Information) and Table S4 (Supporting Information) exhibited the X-ray diffraction (XRD) patterns and the corresponding Rietveld refinement results of all as-synthesized samples, which proved that the in-situ modification would not destroy the layered structural.[2] The NCM811 precursor exhibited micron-sized secondary spherical particles with a flower-like morphology (Figure S3a, b, Supporting Information). After annealing at 800 °C, pristine NCM811 could be obtained with sphere-like secondary particles (~10 μm) tightly packed from smooth primary particles (Figure S3c, Supporting Information). As expected, the surface of NCM811-LBO

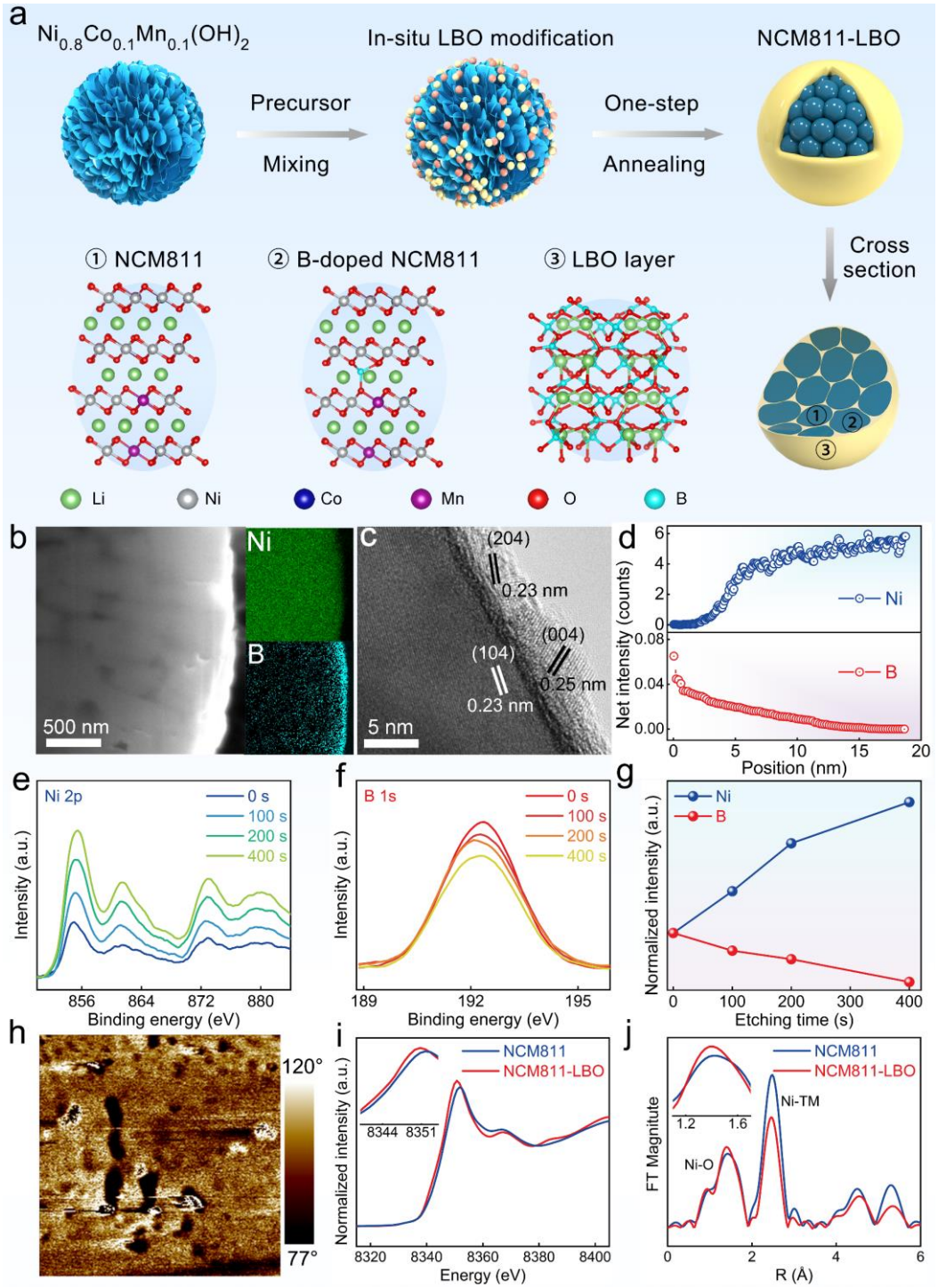

Figure 2. (a) Schematic illustration for the preparation of NCM811-LBO; (b) cross-section SEM image with element mappings (Ni and B) of NCM811-LBO; (c) HRTEM image and (d) TEM-EDS line scanning result for NCM811-LBO; XPS spectra for (e) Ni 2p, (f) B 1s and (g) corresponding normalized results with various argon ion etching time; (h) phase images of LBO detected by PFM technique; (i) XANES and (j) EXAFS spectra at Ni-edge for NCM811 and NCM811-LBO.

become obscure (Figure S3d, Supporting Information), implying the successful surface decoration after LBO treatment. To manifest the piezoelectric property of the coating layer, pure LBO powder was prepared applying the same synthesis conditions as in the coating operation. XRD pattern (Figure S4, Supporting Information) confirmed the as-prepared pure LBO material without any other impurity. Furthermore, piezoelectric force microscope (PFM) was employed to investigate the piezoelectric property of the as-prepared LBO material (Figure 2h; Figure S5a-c, Supporting Information), the high-contrast amplitude (Figure S5c, Supporting Information) and phase images (Figure 2h) manifested the desirable piezoelectric effect.[21] Focused ion beam combined with scanning electron microscope (FIB-SEM) technique was applied to investigate the cross-sectional element distribution of the as-synthesized NCM811-LBO secondary particle. The corresponding energy dispersive X-ray spectroscopy (EDS) mapping of the cross-section structure displayed in Figure 2b and Figure S6 (Supporting Information) obviously demonstrated that H_3BO_3 (HBO) could be in-situ lithiated to LBO with fast Li^+ conductivity and piezoelectric properties under a high temperature of 800 °C. Meanwhile, B^{3+} cations would gradiently incorporate into each primary particle under thermally driven process.

High-resolution transmission electron microscopy (HRTEM) was employed to characterize the microstructure of NCM811-LBO. As could be observed in Figure 2c, a heterogeneous dense layer with a thickness of ~ 5 nm was deposited on the surface of NCM811-LBO. Typically, the interior lattice fringe with an average space of ~ 0.23 nm could be identified to the (104) plane of Ni-rich cathode, and the exterior lattice fringe with a distance of ~ 0.25 nm and ~ 0.23 nm was ascribed to the (004) and (204) plane of LBO decoration layer.[22] Particularly, the improved intensities of Ni element and mitigated B signal with the line scanning depth (Figure 2d, TEM-EDS line scanning images), from another perspective illustrated the successfully LBO encapsulating and B-gradient incorporating in NCM811-LBO. The LBO layer was observed to be ~ 5 nm in thickness (Figure 2c), and the TEM-EDS line scanning image showed that the B signal extended from the secondary particle surface to a depth of ~ 15 nm inside the lattice, thus the B ions were gradiently doped in the range of ~ 10 nm from the lattice surface to interior. X-ray photoelectron spectroscopy (XPS)

characterization was applied to detect the elemental chemical environment of the as-prepared samples (Figure S7, Supporting Information). Representatively, the Ni and B distribution was detected by XPS depth analysis, wherein successive argon ion etching was performed for the NCM811-LBO particles. As shown in Figure 2e-g, B signals mitigated gradually from the surface to the inner bulk with etching time, accompanied with the continuous peak growth for Ni atom, providing a solid evidence for the gradient doping of B cations.

To reveal the influence of B-doping on the valence state of Ni element, X-ray absorption near edge structure (XANES) spectra was collected and the normalized result was shown in Figure 2i. The Ni signal shifted to lower energy for NCM811-LBO compared with that of the pristine material, implying the lowered valence state of Ni,[23] from another viewpoint confirming B element incorporation into the bulk NCM811-LBO. Typically, the lowered valence state of Ni could contribute to higher discharge capacity of NCM811-LBO cathode, which will be discussed in the following electrochemical measurements. The local coordination information of Ni-edge was obtained by the Fourier transform magnitude of extended X-ray absorption fine structure (EXAFS) spectra (Figure 2j). The intensity of first coordination shell (Ni-O) in NCM811-LBO was slightly decreased, again manifesting the lowered Ni valence state. Particularly, the electron configuration of Ni^{3+} was considered as the low spin state $t_2^6e^1$ (Jahn-Teller effect),[24] which could trigger the severe distortion of NiO_6, thus the lowered Ni cations valence state could effectively enhance the structural stability of Ni-rich cathodes.

Firstly, the NCM811 electrodes under different LBO treatment strategies were tested by half cells and compared in Figure S8 (Supporting Information). It is clear that the in-situ LBO modified NCM811 exhibited superior capacity retention than the other electrodes, confirming the collaborative advantage in the electrochemical performances, which was hereafter selected for intensive analysis in the following context. **Figure 3**a demonstrated the NCM811-LBO cathode delivered an initial discharge capacity of 201.2 mAh g^{-1} at 0.1 C (22 mA g^{-1}), with approximate 6.6 mAh g^{-1} higher than its pristine counterpart (194.6 mAh g^{-1}). The increased specific capacity could be attributed to the reduction of Ni valence, providing another solid evidence for B-doping into the tetrahedral position. As observed in Figure 4b-d and Figure S9

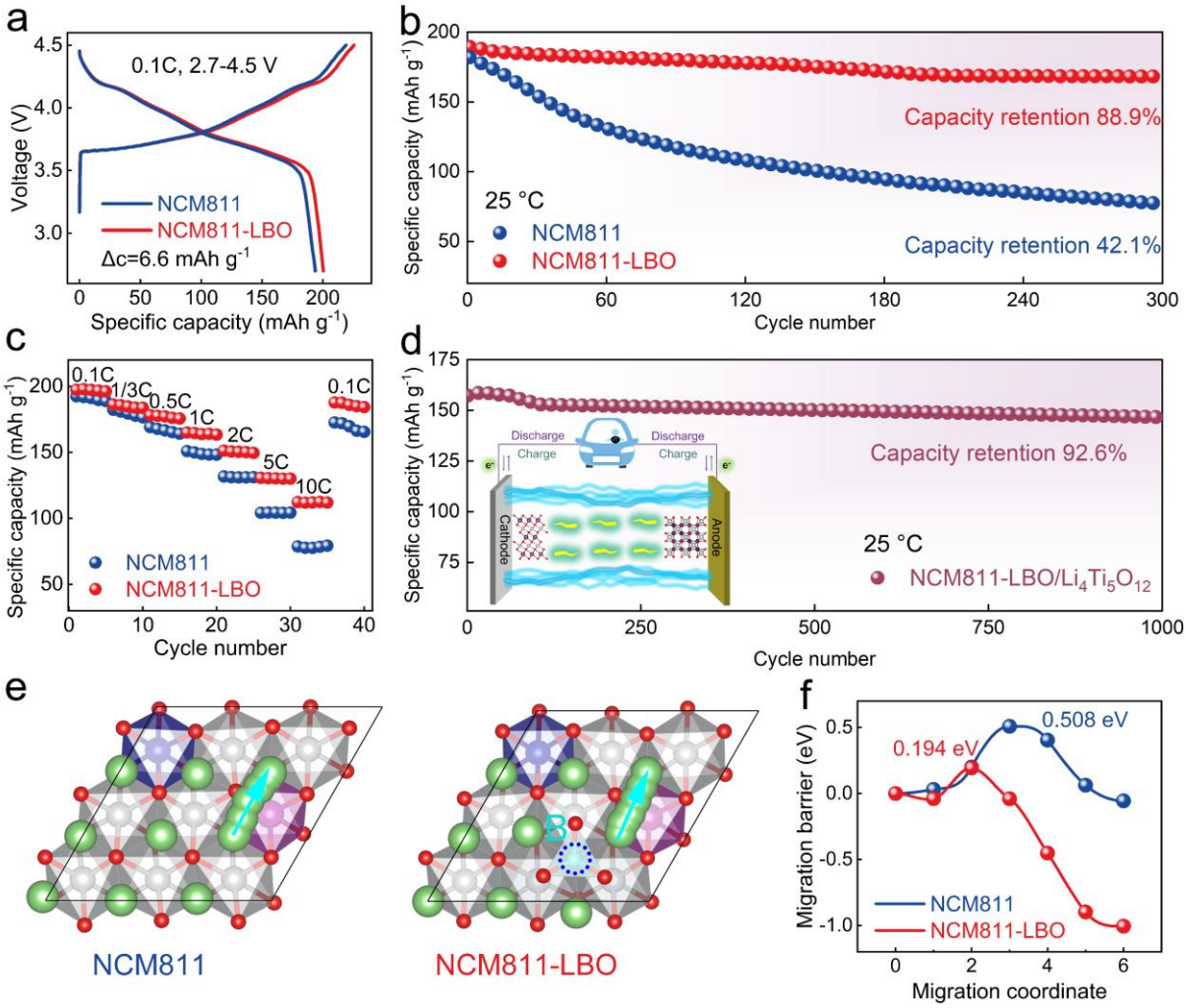

Figure 3. (a) Initial charge-discharge profiles for NCM811 and NCM811-LBO; (b) cycling performances for NCM811 and NCM811-LBO at 1 C under 25 °C; (c) rate performances for NCM811 and NCM811-LBO; (d) cycling performances NCM811-LBO/$Li_4Ti_5O_{12}$ full cell at 0.5 C under 25 °C; (e) theoretical models for Li^+ diffusion paths and (f) corresponding diffusion energy barriers for NCM811 and NCM811-LBO.

(Supporting Information), the electrochemical performances of the modified Ni-rich cathode were obviously improved. After 300 cycles at 25 °C (Figure 3b), the NCM811-LBO cathode could still deliver a reversible capacity of 168.2 mAh g^{-1} with a capacity retention of 88.9% under 1 C, whereas the pristine NCM811 only maintained 77.6 mAh g^{-1} in capacity and 42.1% in capacity retention within the same electrochemical process. The electrochemical performance of NCM811-LBO was found superior compared with the recent reported literatures (Table S5, Supporting Information). The NCM811-LBO cathode was also attained an enhanced capacity retention compared to their pristine counterpart at elevated temperature

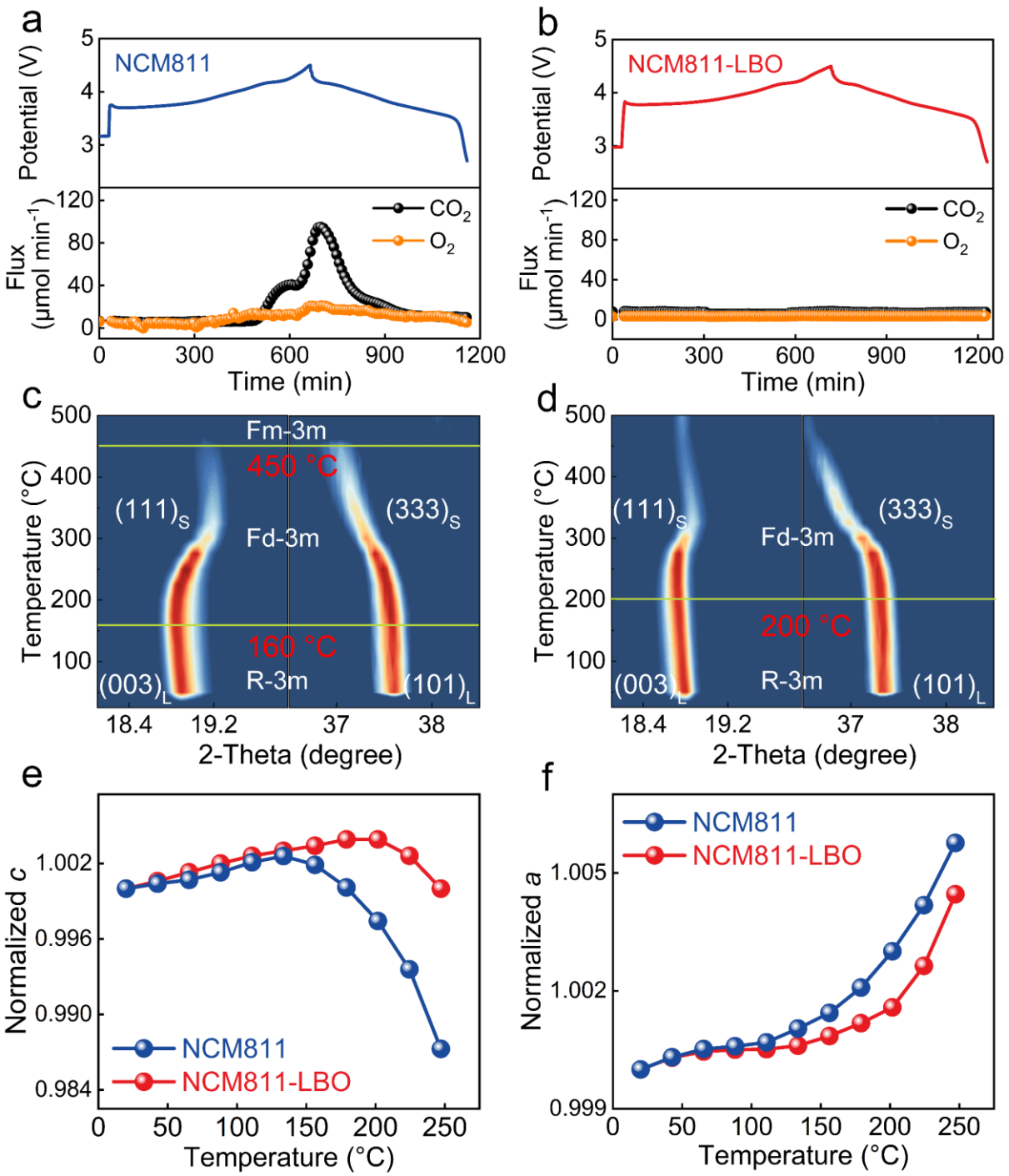

Figure 4. In-situ DEMS measurements for (a) NCM811 and (b) NCM811-LBO; in-situ HT-XRD patterns for (c) NCM811 and (d) NCM811-LBO; normalized evolutions of the lattice parameters of (e) *c* and (f) *a*.

of 50 °C (Figure S9, Supporting Information). Specifically, the NCM811-LBO cathode delivered a high discharge capacity of 112.2 mAh g^{-1} even at the current density of 10 C (Figure 3c), much higher than the NCM811 material (78.6 mAh g^{-1}). Furthermore, the NCM811-LBO/$Li_4Ti_5O_{12}$ full cell retains an excellent capacity of 92.6% after 1000 cycles

under 0.5 C (Figure 3d). The enhanced electrochemical performances and rate capabilities simultaneously elucidated the improved structural stability and Li^+ transport dynamics after in-situ LBO treatment.

The well-maintained structural stability and enhanced phase transition reversibility could be partly explained by the dQ/dV profiles (Figure S10, Supporting Information). Density functional theory (DFT) calculation was employed to investigate the Li^+ diffusion barrier of NCM811 and NCM811-LBO cathodes, respectively. Based on the theoretical model of Li^+ migration pathway in the bulk Ni-rich material (Figure 3e), it manifested that a diffusion barrier drop of 314 meV could be obtained after B incorporation (Figure 3f), partly explained the enhanced Li^+ diffusion kinetics in CV and EIS analysis (Figure S11d-f, Supporting Information) as well as the improved rate performances (Figure 3c). Furthermore, to directly reveal any piezoelectric effect of $Li_2B_4O_7$ on the Li^+ kinetics of Ni-rich cathode, CV profiles under different scan rates as well as rate performances of pristine NCM811, non-piezoelectric LBO-NCM811 and piezoelectric LBO-NCM811 were investigated, and the corresponding results were compared in Figure S12 (Supporting Information). As could be observed in the CV profiles (Figure S12a-c, Supporting Information), the electrode polarization was effectively mitigated after LBO treatment, particularly for the piezoelectric LBO modified electrode. Furthermore, the Li^+ diffusion coefficients could be obtained by fitting the I_p–$v^{1/2}$ line of CV curves (Figure S12d, Supporting Information), which was thus calculated to be 5.05×10^{-11} cm^2 s^{-1} for piezoelectric LBO-NCM811, higher than that of the non-piezoelectric LBO-NCM811 sample (4.28×10^{-11} cm^2 s^{-1}, Figure S12e, Supporting Information), unambiguously providing an obvious proof in the enhanced Li^+ kinetics after piezoelectric LBO treatment. Additionally, the rate performances (Figure S12f, Supporting Information) in piezoelectric LBO-modified NCM811 cathodes also exhibited the most effective improvement, again presenting a solid evidence for the piezoelectric effect of $Li_2B_4O_7$ in boosting the Li^+ kinetics for Ni-rich cathode upon cycling.

In-situ differential electrochemical mass spectrometry (DEMS) was applied to detect the irreversible oxygen redox activities for both NCM811 and NCM811-LBO electrodes upon initial cycle (**Figure 4**a, b). The release of O_2 and CO_2 could be strikingly monitored during

the lithiation of pristine NCM811 (Figure 4a), whereas no obvious gas release was involved in the corresponding curve of NCM811-LBO cathode (Figure 4b). The detected CO_2 could be assigned to the decomposition of carbonate impurities (such as Li_2CO_3) when charged to high potential from 4.0 V to 4.5 V,[25] and the collected O_2 was believed related to the irreversible oxidation and escape of lattice oxygen.[1] The detrimental oxygen release upon repeated cycling would induce irreversible structural transformation and fast capacity fading as well as severe safety concerns.[26] The results herein clearly confirmed that the LBO modification could stabilize the lattice O in Ni-rich cathode, consistent with the above-mentioned theoretical calculations (Figure 1b-e).

In-situ high-temperature XRD (HT-XRD) characterization was carried out to ascertain the structural and thermal stabilities of the delithiated electrodes (Figure 4c-f and Figure S13, Supporting Information). With elevating temperature to ~ 160 °C, the initial layered (R-3m) NCM811 electrode transformed to a disordered spinel structure (Fd-3m), which was indicated by the skewing of $(003)_L$ peak (Figure 4c).[27] Then, it was followed by another phase transformation until the main peaks were well indexed to a cubic rock salt phase (Fm-3m) without other impurities at ~ 450 °C.[28] Comparatively, the corresponding spinel phase transition temperature for NCM811-LBO electrode was increased to ~ 200 °C and the spinel phase remained well even heating up to 500 °C. The phase transition of Ni-rich cathode upon heating was generally induced by the reduction of Ni^{3+}/Ni^{4+} to Ni^{2+}, which could migrate from the octahedral sites in TM layer to the octahedral sites in Li layer upon the reduction process. As a result, the Li^+ diffusion barrier could be increased. Meanwhile, oxygen release from the crystal structure will be inevitably induced to maintain the overall charge neutrality,[28] and the generated oxygen vacancies will further lower the activation barrier for the migration of TM cations, eventually accelerating the phase transitions. The postponed phase transformation unambiguously attested the enhanced structural/thermal stabilities and the lowered oxygen activities in NCM811-LBO electrode. To quantitatively reveal the lattice changes upon heating, the lattice parameters were further obtained by Rietveld refinement of XRD patterns (Figure 4e, f). The initial slight growth of lattice parameter *c* could be ascribed to the lattice expansion under moderate treatment, and the latter process was related to the

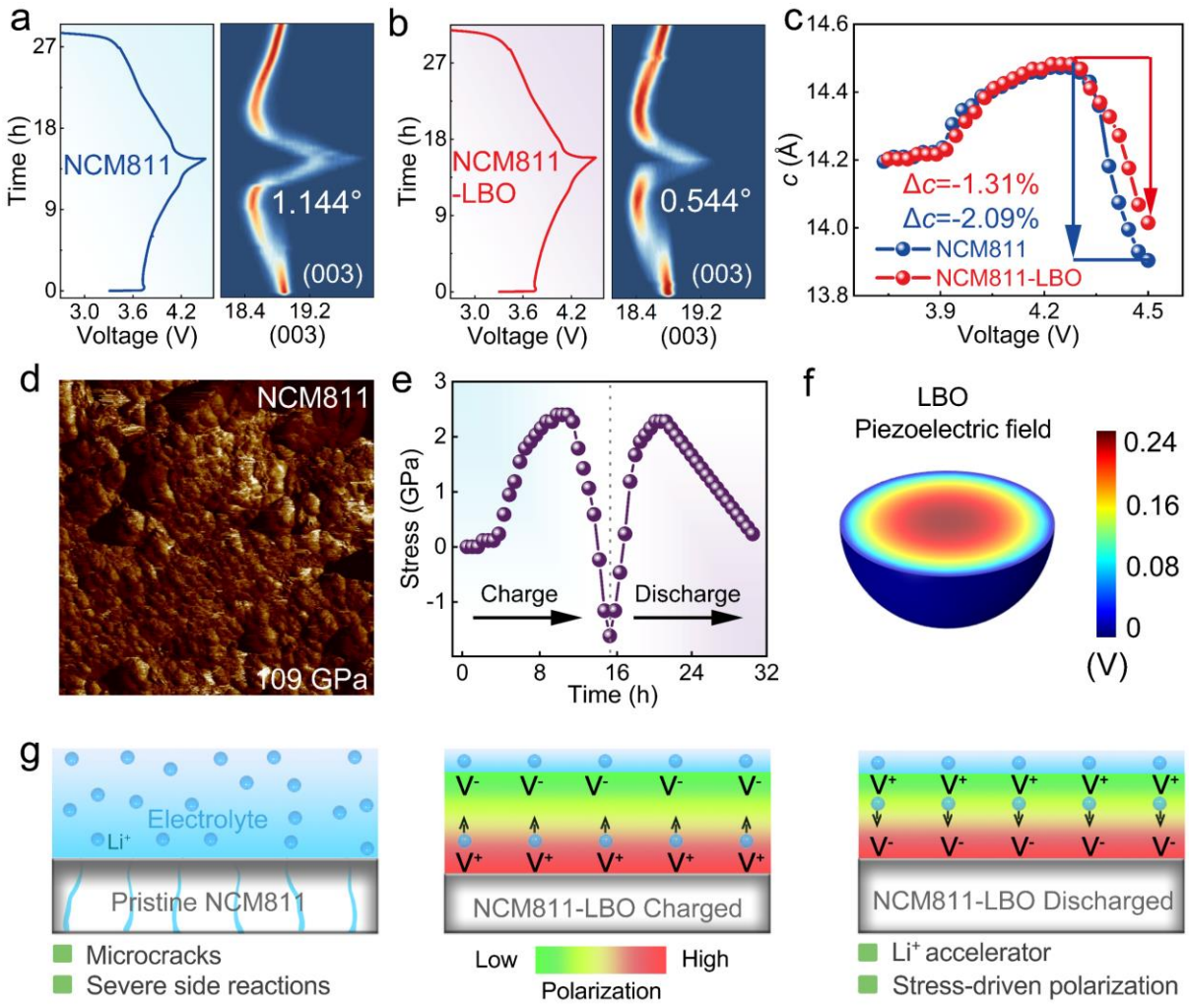

Figure 5. In-situ XRD patterns of (003) peaks in the initial cycle for (a) NCM811 and (b) NCM811-LBO; (c) evolution of lattice parameter *c* for NCM811 and NCM811-LBO; (d) Young's modulus of NCM811 tested by PFM technique; (e) stress curves for NCM811-LBO during initial cycle; (f) finite element analysis of piezoelectric field distribution in LBO layer; (g) schematic illustration of the regulation effect of piezoelectric LBO layer on Li^+ transportation at NCM811 interfacial.

phase transformation and oxygen release.[29] In contrast, the lattice parameter *c* exhibited a larger expansion before degradation, confirming that NCM811-LBO cathode could withhold more *c*-axis expansion than the pristine material. The linear expanding of lattice parameter *a* below 200 °C in Figure 4f could be mainly ascribed to the thermal expansion. Though the *a*-axis increased rather sharply with further temperature elevating, which was induced by the TM ion migration and corresponding phase transformation, the temperature in phase transition for the modified electrode was significantly elevated. The depressed phase

transition and lattice changes in NCM811-LBO sample monitored by the in-situ HT-XRD, unambiguously manifested that the oxygen release and thermal runaway were effectively alleviated under LBO treatment, coinciding with the in-situ DEMS measurements (Figure 4a, b).

In-situ XRD analysis was performed in initial cycle to assess the effect of in-situ LBO construction on structural stability (**Figure 5**a, b; Figure S14a, b, Supporting Information). The lattice parameter *c* underwent a nonlinear evolution composed of gradual increase and sharply degradation (Figure 5c). The *c*-axis expansion under 4.2 V could be attributed to the increase of O─O repulsion due to the Li^+ removal within Li-slab and the contraction above 4.2 V was mainly related to the shrinkage of interlayer distance between NiO_6 sheets, which could be explained by the electron transfer from e_g orbit to 2*p* energy band of O^{2-} during $Ni^{2+/3+/4+}$ oxidation process.[30] The peak shift during H2→H3 phase transition was 1.144° and 0.544° for NCM811 and NCM811-LBO, corresponding to their maximum shrinkages of 2.09% and 1.31% respectively. The alleviated lattice collapse in NCM811-LBO cathodes might be ascribed to the incorporated B^{3+} cations synchronously lowered O 2*p* energy band and acted as pillars under its highly delithiated state. Particularly, suppressed peak shift (1.144°→0.544°) evidently manifested the mitigated stress accumulation and thus partly explained the above-mentioned enhanced electrochemical performances in modified cathodes (Figure 3b-d).

The Young's modulus of pristine NCM811 was detect by atomic force microscopy (AFM) and determined to be 109 GPa (Figure 5d). The strain and stress values of NCM811-LBO in the initial cycle were calculated using formulas S1 and S2 (Supporting Information) and shown in Figure 5e, Figure S15a (Supporting Information). With the transmission of lattice strain of interior Ni-rich particle, the induced force imposed on piezoelectric LBO layer would motivate the additional polarized electric field, which was simulated and shown in Figure 5f and Figure S15b (Supporting Information). The maximum value of polarized potential triggered in NCM811-LBO cathodes was determined to be 0.52 V in the charged state (Figure S15b, Supporting Information). During the discharge process, same maximum potential could be obtained, with the extra voltage of 0.24 V maintained at the end of 1st cycle (Figure 5f). It should be highlighted that the orientation of triggered potential was in accord

with that of Li^+ diffusion upon cycling, which would be favorable for Li^+ kinetics behavior in battery operation.

Based on the above analysis, the schematic diagrams of LBO contribution to Ni-rich electrode were demonstrated in Figure 5g. The pernicious strain in pristine NCM811 will lead to internal microcracks prolonged to the external surface, wherein the infiltrated electrolyte inevitably leads to severe erosion on electrode material. Nevertheless, the LBO piezoelectric layer would play positive roles through rationally transforming the strain-stress of NCM811, particularly that the polarized potential induced in LBO compound was of the same orientation with that of external electric field upon cycling process, acting as a local accelerator to promote Li^+ diffusion at electrolyte-cathode interface. Simultaneously, the improved Li^+ kinetics could depress the stress-strain accumulation through lowering the interfacial energy barrier and eventually elevating the electrochemical performances for the Ni-rich cathodes.

In-situ Raman spectra for NCM811 and NCM811-LBO cathodes in the first cycle were collected and analyzed in **Figure 6**a-d. Two peaks appeared at 483 and 567 cm^{-1}, which were assigned to the typical E_g and A_{1g} modes for TM─O symmetrical stretching and O─TM─O bending vibrations in layered structure (R-3m space group).[31] Further normalized analysis in the intensity evolutions for the E_g and A_{1g} revealed a prominent degeneration upon charging process, which declined more dramatically in NCM811 cathode. The peak degradation manifested the weakened TM─O and O─TM─O bonds, ineluctably accompanied by the structure degradation and lattice oxygen release from the surface structure. The above-mentioned in-situ Raman spectroscopic analysis provided solid evidence that LBO construction could effectually restrain the oxygen release. Finite element analysis was conducted to demonstrate the stress-strain distribution in NCM811 and NCM811-LBO secondary particles under different voltages, with cross-sectional mappings shown in Figure 6e, f. Clearly, the NCM811 cathode showed a larger stress distribution, which was obviously alleviated in NCM811-LBO secondary particles.[32] This discrepancy could be mainly attributed to the in-situ LBO construction, effectively mitigating the stress accumulation of Ni-rich cathode through unique piezoelectric effect.

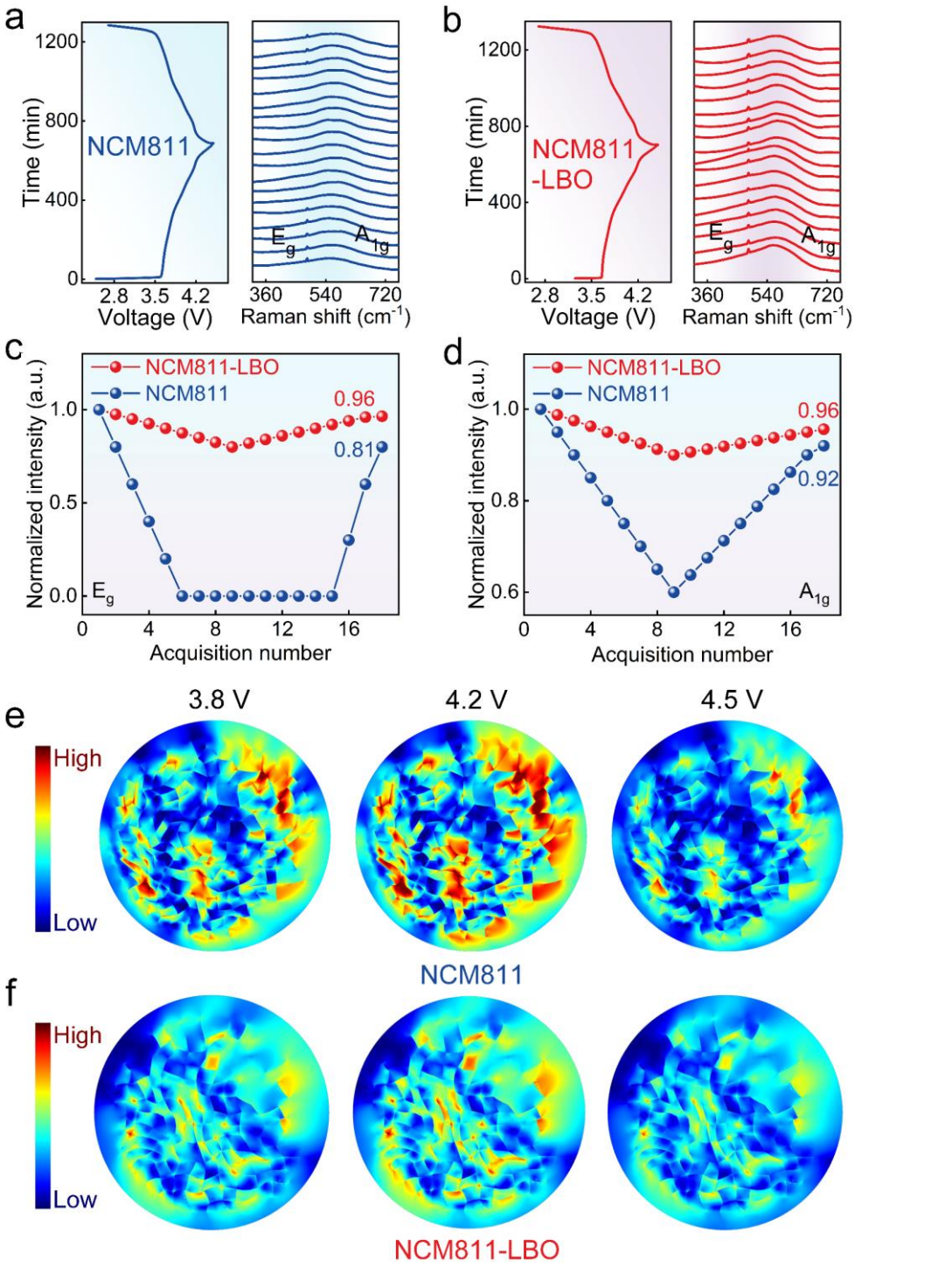

Figure 6. In-situ Raman spectra for (a) NCM811, (b) NCM811-LBO; evolution of integrated intensities for (c) E_g and (d) A_{1g} bands in NCM811 and NCM811-LBO as a function of spectral acquisition number; tension stress distribution for (e) NCM811 and (f) NCM811-LBO particles at different voltage.

Figure S16a-c (Supporting Information) presented the XRD patterns with magnified (003) peak for the NCM811 and NCM811-LBO cathodes before and after 200 cycles. Herein the

slighter (003) peak change in NCM811-LBO indicated that the electrode polarization was effectively weakened,[33] corresponding with the previous *dQ/dV* analysis (Figure S10, Supporting Information). As observed in the topographies of NCM811 and NCM811-LBO cathodes after 200 cycles (Figure S16d, e, Supporting Information), the reduced intracrystalline microcracks providing solid evidence of the structural stability enhancement by LBO modification. HRTEM images were collected to compare the microstructure evolutions of NCM811 and NCM811-LBO cathodes after 200 cycles (Figure S16f, g, Supporting Information). The fairly remained LBO coating layer and unchanged inner layered structural the HRTEM results confirmed that the LBO could stabilize the surface structure of Ni-rich cathode.[34] Elemental mapping images were also obtained for NCM811-LBO **(**Figure S16h, Supporting Information**)**, the homogeneous element distribution could be observed even after 200 cycles, from another viewpoint confirming the strong compatibility between the bulk NCM811 and LBO coating layer. XPS surface analysis was further performed for NCM811 and NCM811-LBO after 200 cycles to observe the surface chemical environment (Figure S17, Supporting Information). The reduction of fluoride (F)-contained compound on NCM811-LBO electrode surface indicated the effectively inhibited generation of CEI films by in situ LBO construction,[35] consistent with the previous EIS (Figure S11a-c, Supporting Information) and HRTEM analysis (Figure S16f, g, Supporting Information). The investigations established herein clearly manifested that the piezoelectric LBO coating could not only suppress the intergranular microcracks and adverse evolution of structural degradation, but also stabilize the near-surface microstructure of Ni-rich cathode to enhance its electrochemical cyclabilities.

3. Conclusions

In this work, heterogeneous B^{3+} cations with high binding energy to lattice O were gradiently incorporated into each primary particle accompanied with the piezoelectric LBO layer encapsulated on the secondary particle surface of polycrystalline NCM811 cathode, aiming to synchronously improve their structural and electrochemical performances through a facile in-situ construction method. The as-prepared NCM811-LBO electrode could retain 88.9% of its initial discharge capacity after 300 cycles under a current density of 1 C, obviously

superior than its pristine counterpart (63.2%). Furthermore, the NC811-LBO/$Li_4Ti_5O_{12}$ full cell achieved 92.6% capacity retention after 1000 cycles under 0.5 C. Multi-scale in/ex-situ experimental characterizations combined with theoretical calculation and finite element analysis elucidated the excellent structural stability in LBO modified samples. The remarkably improved cycling capability and structural stability of the modified cathode could be attributed to the following synergistic contributions: (1) the incorporated B^{3+} cations effectively reduced TM─O covalence and the O atom electronegativity to suppress lattice O escape; (2) the unique doping site of B cations (tetrahedral position in lithium layer) afforded pillar effect in highly delithiated Ni-rich cathodes and thus validly stabilized the crystal structure; (3) the piezoelectric LBO decorator in-situ mitigated the noxious stress from internal materials and accelerated Li^+ diffusion at the cathode-electrolyte interface upon cycling; (4) the deposited LBO layer served as a physical separator to ameliorate the interfacial instability through alleviating possible side-reactions between electrode and electrolyte. The synchronous modification of gradient B-incorporation and uniform piezoelectric LBO-decoration for NCM811 cathode herein not only provides a guidance in manipulating the internal structure and interface stability for ultra-high voltage Ni-rich cathode, but also broadens a new insight for the design and development of energy storage and conversion systems.

Supporting Information

Supporting Information is available from the Wiley Online Library or from the author.

Acknowledgments

This work was supported by the National Natural Science Foundation of China (52072112, 51672069), the Zhongyuan Thousand Talents Program of Henan Province (ZYQR201912155), the Henan Overseas Expertise Introduction Center for Discipline Innovation (CXJD2021003), the Program for Innovative Research Team in Science and Technology in the University of Henan Province (20IRTSTHN012), and Science and Technology Development Project of Henan Province (202102210105, 192102210235).

Conflict of Interest

The authors declare no conflict of interest.

Data Availability Statement

Data available on request from the authors.

Received: ((will be filled in by the editorial staff))
Revised: ((will be filled in by the editorial staff))
Published online: ((will be filled in by the editorial staff))

References

[1] Y. Huang, Y. Zhu, H. Fu, M. Ou, C. Hu, S. Yu, Z. Hu, C. T. Chen, G. Jiang, H. Gu, H. Lin, W. Luo, Y. Huang, *Angew. Chem. Int. Ed.* **2021**, *60*, 4682.

[2] Y. G. Zou, H. Mao, X. H. Meng, Y. H. Du, H. Sheng, X. Yu, J. L. Shi, Y. G. Guo, *Angew. Chem. Int. Ed.* **2021**, *60*, 26535.

[3] H. H. Ryu, N. Y. Park, T. C. Noh, G. C. Kang, F. Maglia, S. J. Kim, C. S. Yoon, Y. K. Sun, *ACS Energy Lett.* **2020**, *6*, 216.

[4] J. Li, A. Manthiram, *Adv. Energy Mater.* **2019**, *9*, 1902731.

[5] H. Yu, Y. Cao, L. Chen, Y. Hu, X. Duan, S. Dai, C. Li, H. Jiang, *Nat. Commun.* **2021**, *12*, 4564.

[6] C. Xu, K. Marker, J. Lee, A. Mahadevegowda, P. J. Reeves, S. J. Day, M. F. Groh, S. P. Emge, C. Ducati, B. Layla Mehdi, C. C. Tang, C. P. Grey, *Nat. Mater.* **2021**, *20*, 84.

[7] S. Li, G. Qian, X. He, X. Huang, S. J. Lee, Z. Jiang, Y. Yang, W. N. Wang, D. Meng, C. Yu, J. S. Lee, Y. S. Chu, Z. F. Ma, P. Pianetta, J. Qiu, L. Li, K. Zhao, Y. Liu, *Nat. Commun.* **2022**, *13*, 704.

[8] a) X. D. Zhang, J. L. Shi, J. Y. Liang, Y. X. Yin, J. N. Zhang, X. Q. Yu, Y. G. Guo, *Adv. Mater.* **2018**, *30*, 1801751; b) S. Li, Z. Yao, J. Zheng, M. Fu, J. Cen, S. Hwang, H. Jin, A. Orlov, L. Gu, S. Wang, Z. Chen, D. Su, *Angew. Chem. Int. Ed.* **2020**, *59*, 22092.

[9] U. H. Kim, G. T. Park, B. K. Son, G. W. Nam, J. Liu, L. Y. Kuo, P. Kaghazchi, C. S. Yoon, Y. K. Sun, *Nat. Energy* **2020**, *5*, 860.

[10] a) H. H. Sun, U. H. Kim, J. H. Park, S. W. Park, D. H. Seo, A. Heller, C. B. Mullins, C. S.

Yoon, Y. K. Sun, *Nat. Commun.* **2021**, *12*, 6552; b) M. Yoon, Y. Dong, J. Hwang, J. Sung, H. Cha, K. Ahn, Y. Huang, S. J. Kang, J. Li, J. Cho, *Nat. Energy* **2021**, *6*, 362.

[11] X. Fan, X. Ou, W. Zhao, Y. Liu, B. Zhang, J. Zhang, L. Zou, L. Seidl, Y. Li, G. Hu, C. Battaglia, Y. Yang, *Nat. Commun.* **2021**, *12*, 5320.

[12] L. Xiang, D. Ren, H. Hungjen, X. Feng, G. L. Xu, M. Zhuang, G. Han, L. Lu, X. Han, Z. Chu, *Joule* **2018**, *2*, 2047.

[13] Z. Dai, J. Wang, H. Zhao, Y. Bai, *Adv. Sci.* **2022**, 2200622.

[14] S. Yin, W. Deng, J. Chen, X. Gao, G. Zou, H. Hou, X. Ji, *Nano Energy* **2021**, *83*, 105854.

[15] a) F. Wu, N. Liu, L. Chen, Y. Su, G. Tan, L. Bao, Q. Zhang, Y. Lu, J. Wang, S. Chen, J. Tan, *Nano Energy* **2019**, *59*, 50; b) A. Gomez, Martin, F. Reissig, L. Frankenstein, M. Heidbüchel, M. Winter, T. Placke, R. Schmuch, *Adv. Energy Mater.* **2022**, *12*, 2103045.

[16] Y. J. Guo, P. F. Wang, Y. B. Niu, X. D. Zhang, Q. Li, X. Yu, M. Fan, W. P. Chen, Y. Yu, X. Liu, Q. Meng, S. Xin, Y. X. Yin, Y. G. Guo, *Nat. Commun.* **2021**, *12*, 5267.

[17] M. Jiang, D. L. Danilov, R. A. Eichel, P. H. L. Notten, *Adv. Energy Mater.* **2021**, *11*, 2103005.

[18] a) C. H. Jung, D. H. Kim, D. Eum, K. H. Kim, J. Choi, J. Lee, H. H. Kim, K. Kang, S. H. Hong, *Adv. Funct. Mater.* **2021**, *31*, 2010095; b) B. Li, H. Yan, J. Ma, P. Yu, D. Xia, W. Huang, W. Chu, Z. Wu, *Adv. Funct. Mater.* **2014**, *24*, 5112.

[19] D. H. Kim, J. H. Song, C. H. Jung, D. Eum, B. Kim, S. H. Hong, K. Kang, *Adv. Energy Mater.* **2022**, *12*, 2200136.

[20] S. Jamil, G. Wang, L. Yang, X. Xie, S. Cao, H. Liu, B. Chang, X. Wang, *J. Mater. Chem. A* **2020**, *8*, 21306.

[21] S. Xia, Y. Zhao, J. Yan, J. Yu, B. Ding, *ACS Nano* **2021**, *15*, 3161.

[22] Y. Charles, Blin, K. Nemoto, N. Zettsu, K. Teshima, *J. Mater. Chem. A* **2020**, *8*, 20979.

[23] X. Liu, G. L. Xu, L. Yin, I. Hwang, Y. Li, L. Lu, W. Xu, X. Zhang, Y. Chen, Y. Ren, C. J. Sun, Z. Chen, M. Ouyang, K. Amine, *J. Am. Chem. Soc.* **2020**, *142*, 19745.

[24] W. Lee, S. Muhammad, T. Kim, H. Kim, E. Lee, M. Jeong, S. Son, J. H. Ryou, W. S. Yoon, *Adv. Energy Mater.* **2018**, *8*, 1701788.

[25] J. Sun, C. Sheng, X. Cao, P. Wang, P. He, H. Yang, Z. Chang, X. Yue, H. Zhou, *Adv.*

Funct. Mater. **2021**, *32*, 2110295.

[26] Q. Zhang, X. Liu, H. Li, Z. Guo, T. Bian, X. Zhu, N. Zhan, Y. Zhao, *Small* **2022**, *18*, 2106395.

[27] Y. Li, X. Liu, L. Wang, X. Feng, D. Ren, Y. Wu, G. Xu, L. Lu, J. Hou, W. Zhang, Y. Wang, W. Xu, Y. Ren, Z. Wang, J. Huang, X. Meng, X. Han, H. Wang, X. He, Z. Chen, K. Amine, M. Ouyang, *Nano Energy* **2021**, *85*, 105878.

[28] E. Lee, S. Muhammad, T. Kim, H. Kim, W. Lee, W. S. Yoon, *Adv. Sci.* **2020**, *7*, 1902413.

[29] J. Hou, X. Feng, L. Wang, X. Liu, A. Ohma, L. Lu, D. Ren, W. Huang, Y. Li, M. Yi, Y. Wang, J. Ren, Z. Meng, Z. Chu, G. L. Xu, K. Amine, X. He, H. Wang, Y. Nitta, M. Ouyang, *Energy Storage Mater.* **2021**, *39*, 395.

[30] W. Li, H. Y. Asl, Q. Xie, A. Manthiram, *J. Am. Chem. Soc.* **2019**, *141*, 5097.

[31] H. Huang, Z. Li, S. Gu, J. Bian, Y. Li, J. Chen, K. Liao, Q. Gan, Y. Wang, S. Wu, Z. Wang, W. Luo, R. Hao, Z. Wang, G. Wang, Z. Lu, *Adv. Energy Mater.* **2021**, *11*, 2101864.

[32] S. Lou, Q. Liu, F. Zhang, Q. Liu, Z. Yu, T. Mu, Y. Zhao, J. Borovilas, Y. Chen, M. Ge, X. Xiao, W. K. Lee, G. Yin, Y. Yang, X. Sun, J. Wang, *Nat. Commun.* **2020**, *11*, 5700.

[33] M. Fan, X. Chang, Y. J. Guo, W. P. Chen, Y. X. Yin, X. Yang, Q. Meng, L. J. Wan, Y. G. Guo, *Energy Environ. Sci.* **2021**, *14*, 1461.

[34] C. Wang, L. Han, R. Zhang, H. Cheng, L. Mu, K. Kisslinger, P. Zou, Y. Ren, P. Cao, F. Lin, H. L. Xin, *Matter* **2021**, *4*, 2013.

[35] K. J. Park, H. G. Jung, L. Y. Kuo, P. Kaghazchi, C. S. Yoon, Y. K. Sun, *Adv. Energy Mater.* **2018**, *8*, 1801202